

Measurement of the transverse polarization of electrons emitted in neutron decay – nTRV experiment

K. Bodek^{1*} and A. Kozela²

¹ M. Smoluchowski Institute of Physics, Jagiellonian University, Cracow, Poland

² H. Niewodniczański Institute of Nuclear Physics, Polish Academy of Sciences, Cracow, Poland

* kazimierz.bodek@uj.edu.pl

June 8, 2021



Review of Particle Physics at PSI
doi:[10.21468/SciPostPhysProc.2](https://doi.org/10.21468/SciPostPhysProc.2)

Abstract

This paper recalls the main achievements of the nTRV experiment which measured two components of the transverse polarization (σ_{T_1} , σ_{T_2}) of electrons emitted in the β -decay of polarized, free neutrons and deduced two correlation coefficients, R and N , that are sensitive to physics beyond the Standard Model. The value of time-reversal odd coefficient R , $0.004 \pm 0.012 \pm 0.005$, significantly improved limits on the relative strength of imaginary scalar coupling constant in the weak interaction. The value obtained for the time-reversal even correlation coefficient N , $0.067 \pm 0.011 \pm 0.004$, agrees with the Standard Model expectation, providing an important sensitivity test of the electron polarimeter. One of the conclusions of this pioneering experiment was that the transverse electron polarization in the neutron β -decay is worth more systematic exploring by measurements of yet experimentally not attempted correlation coefficients such as H , L , S , U and V . This article presents a brief outlook on that questions.

15.1 Introduction

Nuclear and neutron beta decay have played a central role in the development of the weak interaction theory. Among the empirical foundations of the electroweak sector of the Standard Model (SM), the assumptions of maximal parity violation, the vector and axial-vector character, and massless neutrinos are directly linked to nuclear and neutron beta decay experiments. Beta decay theory was firmly established about six decades ago and became a part of the SM. It describes the semi-leptonic and strangeness-conserving processes in the 1-st particle generation mediated by charged W -boson exchange. Despite the neutrino masses have been shown to be finite – beta decay experiments with increasing precision still confirm the first two assumptions. Nevertheless, many open questions remain such as the origin of parity violation, the hierarchy of fermion masses, the number of particle generations, the mechanism of CP violation, and the unexplained large number of parameters of the theory. A major breakthrough would be a discovery of new CP- or T-violation sources different from the CKM matrix induced mechanism reported for heavier systems in [1, 2]. Especially interesting are processes in the systems built of light quarks with vanishingly small contributions of the CKM matrix mechanism such as nuclear beta decay. Therein, experiments with free neutrons play a particularly important role since their interpretation is free of complications connected with nuclear and atomic structure. In addition, the effects of $p - e$ electromagnetic interaction in the final state,

41 which can mimic T-violation, are small and can be calculated with a relative precision better
42 than 1% [3–5].

43 The nTRV project at PSI, was the first experimental search for the real and imaginary parts
44 of the scalar and tensor couplings using the measurement of the transverse polarization of
45 electrons emitted in the free neutron decay. There are very few measurements of this observ-
46 able in general [6,7], and only two in nuclear beta decays. One of them, for the ^8Li system [8],
47 provides the most stringent limit on the tensor coupling constants of the weak interaction.

48 According to [9], the decay rate distribution from polarized neutrons as a function of elec-
49 tron energy (E) and momentum (\mathbf{p}) is proportional to:

$$\omega(\mathbf{J}, \hat{\boldsymbol{\sigma}}, E, \mathbf{p}) \propto 1 + \frac{\langle \mathbf{J} \rangle}{J} \cdot \left(A \frac{\mathbf{p}}{E} + N \hat{\boldsymbol{\sigma}} + R \frac{\mathbf{p} \times \hat{\boldsymbol{\sigma}}}{E} \right) + \dots \quad (15.1)$$

50 where $\frac{\langle \mathbf{J} \rangle}{J}$ ($J = |\mathbf{J}|$) is the neutron polarization, $\hat{\boldsymbol{\sigma}}$ is the unit vector onto which the electron spin
51 is projected, and A is the beta decay asymmetry parameter. N and R are correlation coefficients
52 which, for neutron decay with usual SM assumptions: $C_V = C'_V = 1$, $C_A = C'_A = \lambda = -1.276$ [10]
53 and allowing for a small admixture of scalar and tensor couplings C_S , C_T , C'_S , C'_T , can be
54 expressed as:

$$N = -0.218 \cdot \text{Re}(\mathfrak{S}) + 0.335 \cdot \text{Re}(\mathfrak{T}) - \frac{m}{E} \cdot A, \quad (15.2)$$

$$R = -0.218 \cdot \text{Im}(\mathfrak{S}) + 0.335 \cdot \text{Im}(\mathfrak{T}) - \frac{m}{137p} \cdot A, \quad (15.3)$$

55 where $\mathfrak{S} \equiv (C_S + C'_S)/C_V$, $\mathfrak{T} \equiv (C_T + C'_T)/C_A$ and m is the electron mass. The R correlation coef-
56 ficient vanishes in the lowest order SM calculations. It becomes finite if final state interactions
57 are included, $R_{FSI} \approx -\frac{m}{137p} \cdot A \approx 0.0006$, below the sensitivity of this experiment. A larger
58 value of R would provide evidence for the existence of exotic couplings, and a new source
59 of time reversal violation (TRV). Using Mott polarimetry, both transverse components of the
60 electron polarization can be measured simultaneously: σ_{T_2} perpendicular to the decay plane
61 defined by the neutron spin and electron momentum associated with R , and σ_{T_1} contained in
62 the decay plane and associated with N . The SM value of N is finite and well within reach of
63 this experiment. Its determination provides an important test of the experimental sensitivity.

64 15.2 Experiment

65 The experiment was performed at the FUNSPIN beam line [11] at the neutron source SINQ of
66 the Paul Scherrer Institute, Villigen, Switzerland. A detailed description of the design, oper-
67 ation and performance of the Mott polarimeter can be found in [12]. Only a short overview
68 is presented here. The final result comprises independent analyses of four data collection pe-
69 riods, featuring different basic conditions such as beam polarization, Mott foil thickness and
70 acquired statistics.

71 The Mott polarimeter consisted of two identical modules, arranged symmetrically on either
72 side of the neutron beam (Figure 15.1). The whole structure was mounted inside a large-
73 volume dipole magnet providing a homogeneous vertical spin-holding field of 0.5 mT within
74 the beam fiducial volume. An RF-spin flipper (not shown in Figure 15.1) was used to reverse
75 the orientation of the neutron beam polarization at regular time intervals, typically every 16 s.
76 Going outwards from the beam, each module consisted of a multi-wire proportional chamber
77 (MWPC) for electron tracking, a removable Mott scatterer (1-2 μm Pb layer evaporated on a
78 2.5 μm thick mylar foil) and a scintillator hodoscope to measure the electron energy.

79 A 1-cm-thick plastic scintillator, used for the electron energy reconstruction, had a reso-
80 lution of 33 keV at 500 keV. The asymmetry of the light signal collected at the ends of the
81 scintillator slab was used to determine the vertical hit position with a resolution of about 6

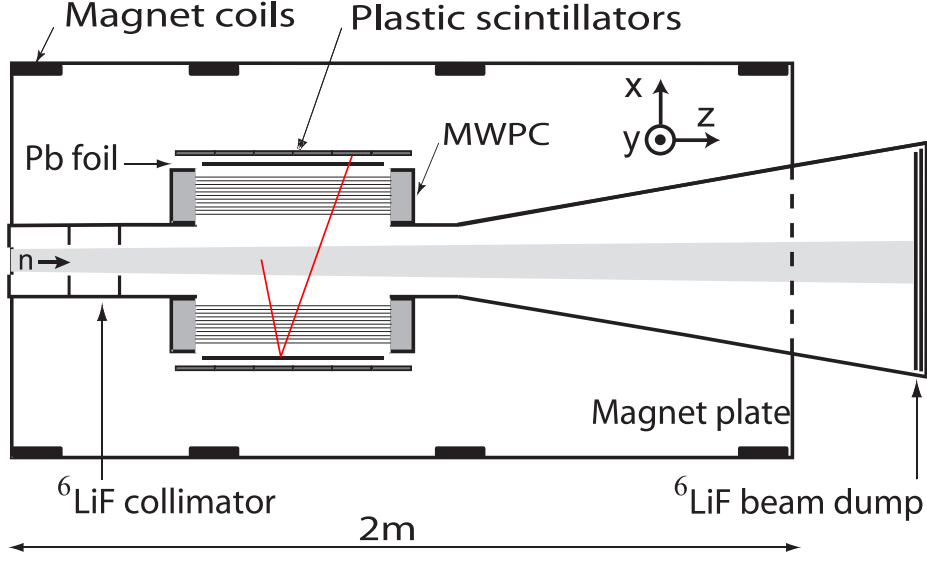


Figure 15.1: Schematic top view of the experimental setup. A sample projection of an electron V-track event is indicated [13].

82 cm: the segmentation (10 cm) of the hodoscope in the horizontal direction provided a crude
 83 estimate of the z-coordinate. Matching the information from the precise track reconstruction
 84 in the MWPC with that from the scintillator hodoscope reduced background and random co-
 85 incidences considerably.

86 A 1.3-m-long multi-slit collimator defined the beam cross section to $4 \times 16 \text{ cm}^2$ at the en-
 87 trance of the Mott polarimeter. To minimize neutron scattering and capture, the entire beam
 88 volume, from the collimator to the beam dump, was enclosed in a chamber lined with ${}^6\text{Li}$
 89 polymer and filled with pure helium at atmospheric pressure. The total flux of the collimated
 90 beam was typically about 10^{10} neutrons/sec. Thorough investigations of the beam polarization
 91 performed in a dedicated experiment [11] showed a substantial dependence on the position
 92 in the beam fiducial volume. The average beam polarization necessary for the evaluation of
 93 the N - and R -correlation coefficients was extracted from the observed decay asymmetry using
 94 the precisely known [10] beta decay asymmetry parameter $A = -0.1196 \pm 0.0002$. This ap-
 95 proach automatically accounts for the proper integration over the position-dependent beam
 96 density, its polarization and detector acceptance. For this purpose, single track events (only
 97 one reconstructed track segment on the hit scintillator side) were recorded using a dedicated
 98 prescaled trigger. The main event trigger was used to find V-track candidates: events with two
 99 reconstructed segments on one side and one segment accompanied by a scintillator hit on the
 100 opposite side, (see Figure 15.1).

101 The following asymmetries were analyzed to extract the beam polarization, P :

$$\mathcal{E}(\beta, \gamma) = \frac{N^+(\beta, \gamma) - N^-(\beta, \gamma)}{N^+(\beta, \gamma) + N^-(\beta, \gamma)} = P\beta A \cos(\gamma), \quad (15.4)$$

102 where N^\pm are experimental, background-corrected counts of single tracks sorted in 4 bins of
 103 the electron velocity β , and 15 bins of the electron emission angle γ with respect to the neutron
 104 polarization direction. The sign in the superscripts reflects the beam polarization direction.

105 A comparison between the measured and MC simulated energy spectra for direct and Mott-
 106 scattered electrons is shown in Figure 15.2 a and b, respectively. Electronic thresholds are not
 107 included in the simulation – this is why the measured and simulated distributions do not match
 108 at the low energy side.

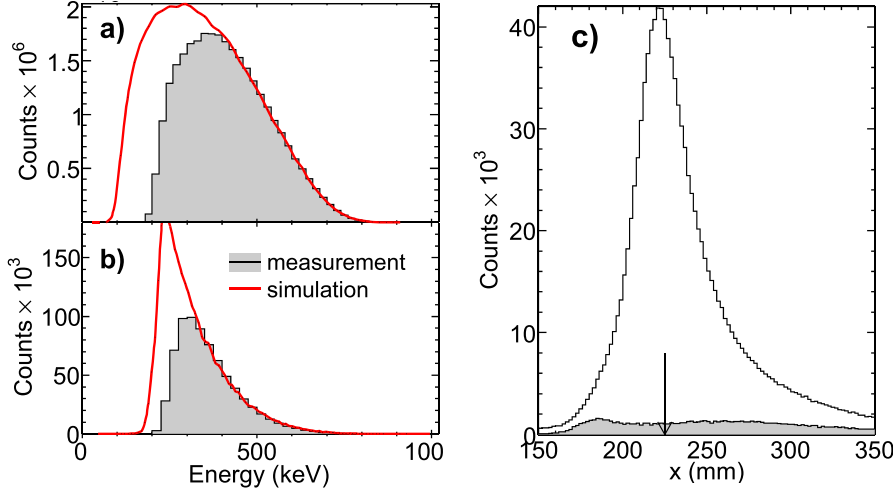


Figure 15.2: Background-corrected experimental energy distributions (shaded areas) of (a) the single-track and (b) V-track events compared with simulations. (c) Background contribution (shaded) to vertex x -coordinate distribution of V-track events. The arrow indicates the Mott foil position [13].

109 Another set of asymmetries was used to extract the N and R correlation coefficients :

$$A(\alpha) = \frac{n^+(\alpha) - n^-(\alpha)}{n^+(\alpha) + n^-(\alpha)}, \quad (15.5)$$

110 where n^\pm represent background-corrected experimental numbers of counts of V-track events,
 111 sorted in 12 bins of α , the angle between electron scattering and neutron decay planes. In
 112 the case of V-track events, beside the background discussed previously, events for which the
 113 scattering took place in the surrounding of the Mott-target provide an additional source of
 114 background. Figure 15.2 c shows the distribution of the reconstructed vertex positions in
 115 the x -direction for data collected with and without the Mott foil. The distribution clearly
 116 peaks at the foil position. This relatively broad distribution is a result of extrapolation of
 117 two electron track segments crossing at relatively small angle ($20^\circ - 60^\circ$). Additionally, the
 118 electron straggling effects contribute to its broadening. The “foil-out” distribution has been
 119 scaled appropriately by a factor deduced from the accumulated neutron beam.

120 It can be shown [12] that

$$A(\alpha) - P\bar{\beta}A\bar{F}(\alpha) = P\bar{S}(\alpha) [\bar{N}\bar{G}(\alpha) + R\bar{\beta}\bar{H}(\alpha)], \quad (15.6)$$

121 where the kinematical factors $\bar{F}(\alpha)$, $\bar{G}(\alpha)$, and $\bar{H}(\alpha)$ represent the average values of the quan-
 122 tities $\hat{\mathbf{J}} \cdot \hat{\mathbf{p}}$, $\hat{\mathbf{J}} \cdot \hat{\boldsymbol{\sigma}}$ and $\hat{\mathbf{J}} \cdot \hat{\mathbf{p}} \times \hat{\boldsymbol{\sigma}}$, respectively, \bar{S} is the effective analyzing power of the electron
 123 Mott scattering, known in the literature as “Sherman function”, and the bar over a letter indi-
 124 cates event-by-event averaging. The term $P\bar{\beta}A\bar{F}$ accounts for the β -decay-asymmetry-induced
 125 nonuniform illumination of the Mott foil. Since the $\bar{\beta}$ and \bar{F} are known precisely from event-
 126 by-event averaging, the uncertainty of this term is dominated by the error of the average beam
 127 polarization P .

128 Mean values of the effective analyzing powers as a function of electron energy, scattering
 129 and incidence angles were calculated using the Geant 4 simulation framework [14], following
 130 guidelines presented in [15, 16]. This approach accounts properly for the atomic structure,
 131 nuclear size effects as well as the effects introduced by multiple scattering in thick foils.

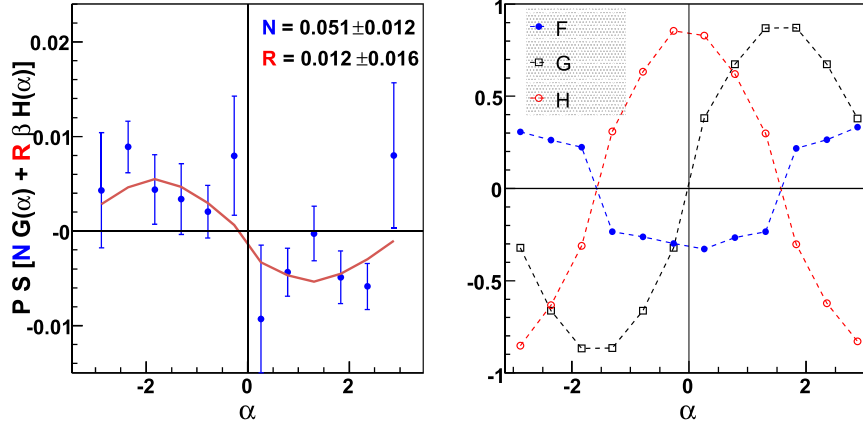


Figure 15.3: Left panel: experimental asymmetries \mathcal{A} corrected for the $P\bar{\beta}A\bar{\mathcal{F}}$ term for the 2007 data set as a function of α (defined in text). The solid line illustrates a two-parameter (N , R) least-square fit to the data. The indicated errors are statistical. Right panel: geometrical factors $\bar{\mathcal{F}}(\alpha)$, $\bar{\mathcal{G}}(\alpha)$ and $\bar{\mathcal{H}}(\alpha)$ for the same data set [13].

132 The systematic uncertainty is dominated by the effects introduced by the background sub-
 133 traction procedure, connected with the choice of the geometrical cuts defining event classes
 134 “from-beam” and “off-beam”. To estimate this effect, the cuts were varied in a range limited
 135 solely by the geometry of the apparatus. Because the radio-frequency of the spin flippers
 136 was a small source of noise in the readout electronics, tiny spin-flipper-correlated dead time
 137 variations were observed. The result was corrected for this effect.

138 The asymmetries as defined in (15.4) and (15.5) have been calculated for events with
 139 energies above the neutron β -decay end-point energy and for events originating outside of
 140 the beam fiducial volume: they were found to be consistent with zero within the statistical
 141 accuracy, which proves that the data were not biased e.g. with a spin-flipper-related false
 142 asymmetry.

143 A fit of the experimental asymmetries \mathcal{A} , corrected for the $P\bar{\beta}A\bar{\mathcal{F}}$ term for the experimental
 144 data set of 2007 is shown in Figure 15.3.

145 From the approximate symmetry of the detector with respect to the transformation $\alpha \rightarrow -\alpha$,
 146 it follows that $\bar{\beta}$, \bar{S} and the factors $\bar{\mathcal{F}}$, $\bar{\mathcal{H}}$ are all symmetric, while $\bar{\mathcal{G}}$ is an antisymmetric function
 147 of α (see Figure 15.3). This allows the extraction of the N coefficient from the expression [12]:

$$148 \quad N \approx \frac{(r-1)}{(r+1)} \cdot \frac{1 - \frac{1}{2}(P\bar{\beta}A\bar{\mathcal{F}})^2}{P\bar{S}\bar{\mathcal{G}}}, \quad r = \sqrt{\frac{n^+(\alpha)n^-(-\alpha)}{n^-(\alpha)n^+(-\alpha)}} \quad (15.7)$$

149 The advantage of this method is that the effect connected with the term $P\bar{\beta}A\bar{\mathcal{F}}$ is suppressed by
 150 a factor of about 60 compared to (15.6). The good agreement between the N values obtained
 151 in both ways enhances confidence in the extracted N and R coefficient values.

152 The systematic uncertainties in the evaluation of the R and N coefficients are dominated by
 153 effects introduced by the background subtraction procedure and the choice of specific values
 154 of the cuts that determine whether an individual event is attributed to “signal” or to “back-
 155 ground”. These effects were systematically studied for all data sets. Additional calibration
 156 measurements were performed to determine the Mott-target mass distribution [17] that can
 157 influence the electron depolarization leading to increased uncertainty of the effective Sherman
 158 function. A detailed description of the data analysis process can be found in [13, 18] together

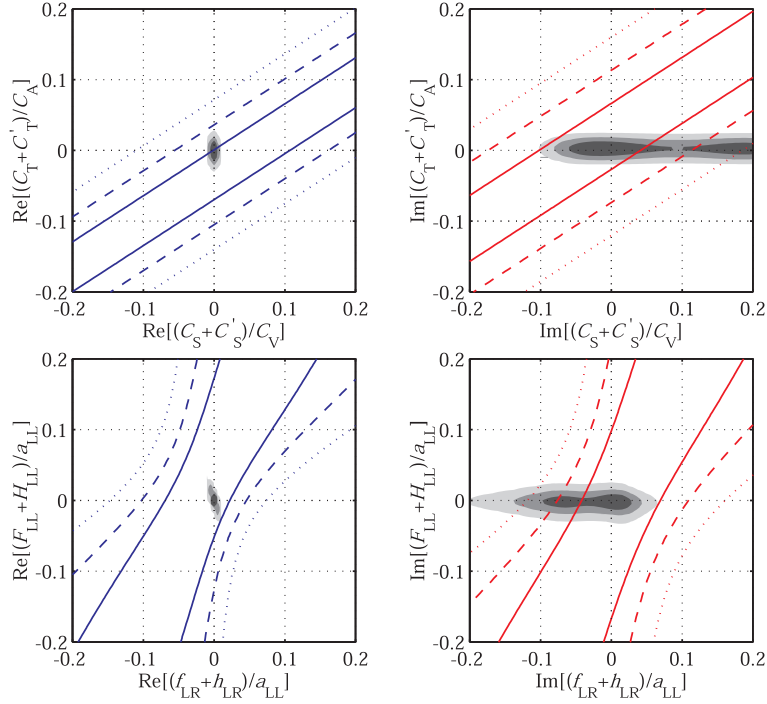


Figure 15.4: Experimental bounds on the scalar vs. tensor normalized couplings (upper) and leptiquark exchange helicity projection amplitudes (lower panels) published in [13]. The gray areas represent the available to date empirical information as listed in [19], while the lines represent the limits resulting from the present experiment. Solid, dashed and dotted lines correspond to 1-, 2- and 3- sigma confidence levels, respectively, in analogy to decreasing intensity of the grey areas.

159 with the final result comprising all available experimental data.

$$R = 0.004 \pm 0.012_{\text{stat}} \pm 0.005_{\text{syst}}, \quad (15.8)$$

$$N = 0.067 \pm 0.022_{\text{stat}} \pm 0.004_{\text{syst}}. \quad (15.9)$$

160 This was the first determination of the N correlation coefficient in β -decay.

161 In Figure 15.4 the new results are included in exclusion plots containing all experimental
 162 information available from nuclear and neutron beta decays as surveyed in [19]. The upper
 163 plots contain the normalized scalar and tensor coupling constants \mathfrak{S} and \mathfrak{T} , while the lower
 164 plots correspond to the helicity projection amplitudes in the leptiquark exchange model, as
 165 defined in [20]. Although the achieved accuracy does not improve the already strong con-
 166 straints on the real part of the couplings (left panels), the result is consistent with the existing
 167 data and increases confidence in the validity of the extraction of R . For the imaginary part
 168 (right panels), the new experimental value of the R coefficient significantly constrains scalar
 169 couplings beyond the limits from all previous measurements. The result is consistent with the
 170 SM.

171 15.3 Outlook – the BRAND project

172 The successful determination of two transverse components of the polarization of electrons
 173 emitted in neutron decay in a pioneering and nearly optimal experiment led to the following
 174 conclusions: (i) it seems quite possible to decrease the systematic uncertainty by an order of
 175 magnitude using existing techniques, (ii) the transverse electron polarization can be studied
 176 in a more systematic way by correlating it with the electron momentum, the neutron spin, and

177 also with the recoil proton momentum by constructing larger and higher acceptance detecting
 178 systems like e.g. proposed by [21] and operating with the highest intensity polarized cold
 179 neutron beam available. In this way, one can study seven correlation coefficients: $H, L, N, R,$
 180 S, U and V where five of them (H, L, S, U, V) have never been experimentally studied:

$$\begin{aligned}
 \omega(E_e, \Omega_e, \Omega_{\bar{\nu}}) &\propto 1 + \\
 &a \frac{\mathbf{p}_e \cdot \mathbf{p}_{\bar{\nu}}}{E_e E_{\bar{\nu}}} + b \frac{m_e}{E_e} + \frac{\langle \mathbf{J} \rangle}{J} \cdot \left[A \frac{\mathbf{p}_e}{E_e} + B \frac{\mathbf{p}_{\bar{\nu}}}{E_{\bar{\nu}}} + D \frac{\mathbf{p}_e \times \mathbf{p}_{\bar{\nu}}}{E_e E_{\bar{\nu}}} \right] + \\
 &\boldsymbol{\sigma}_{\perp} \cdot \left[H \frac{\mathbf{p}_{\bar{\nu}}}{E_{\bar{\nu}}} + L \frac{\mathbf{p}_e \times \mathbf{p}_{\bar{\nu}}}{E_e E_{\bar{\nu}}} + N \frac{\langle \mathbf{J} \rangle}{J} + R \frac{\langle \mathbf{J} \rangle \times \mathbf{p}_e}{J E_e} + \right. \\
 &\left. S \frac{\langle \mathbf{J} \rangle}{J} \frac{\mathbf{p}_e \cdot \mathbf{p}_{\bar{\nu}}}{E_e E_{\bar{\nu}}} + U \mathbf{p}_{\bar{\nu}} \frac{\langle \mathbf{J} \rangle \cdot \mathbf{p}_e}{J E_e E_{\bar{\nu}}} + V \frac{\mathbf{p}_{\bar{\nu}} \times \langle \mathbf{J} \rangle}{J E_{\bar{\nu}}} \right], \tag{15.10}
 \end{aligned}$$

181 where $\boldsymbol{\sigma}_{\perp}$ represents a unit vector perpendicular to the electron momentum \mathbf{p}_e and $J = |\mathbf{J}|$.
 182 $\mathbf{p}_{\bar{\nu}}$ and $E_{\bar{\nu}}$ are the antineutrino momentum and energy, respectively.

183 The coefficients relating the transverse electron polarization to \mathbf{p}_e , $\mathbf{p}_{\bar{\nu}}$ and \mathbf{J} have several
 184 interesting features. They vanish for the SM weak interaction, and reveal the variable size
 185 of the electromagnetic contributions. For H and N , the electromagnetic contributions are of
 186 the order of 0.06, which can be used for an internal sensitivity check of the Mott polarimeter.
 187 Finally, the dependence on the real and imaginary parts of the scalar and tensor couplings
 188 alternates exclusively from one correlation coefficient to another with varying sensitivity. This
 189 feature allows a complete set of constraints to be determined from the neutron decay alone.

190 The idea of implementing such a complex measurement was proposed in [22]. An updated
 191 version of the measurement can be found in [23]. Presently, the first test run devoted to the
 192 verification of the applied detectors and techniques has been completed on the PF1B cold
 193 neutron beam at the Laue Langevin Institute in Grenoble, France (ILL).

194 15.4 EFT parameterization

195 To bridge the classical β -decay formalism with high-energy physics and permit sensitivity com-
 196 parison of low-energy charged-current observables with measurements carried out at high-
 197 energy colliders, the model-independent effective field theory (EFT) framework is employed.
 198 The effective nucleon-level couplings C_i, C'_i ($i \in [V, A, S, T]$) can be generally expressed as
 199 combinations of the quark-level parameters $\epsilon_i, \tilde{\epsilon}_i$ ($i \in [L, R, S, T]$) [25]. The imaginary parts
 200 of the scalar and tensor couplings parameterize CP-violating contributions. The high energy
 201 BSM physics process that can be compared with β -decay experiments is the cross section for
 202 electrons and missing transverse energy (MET) in $pp \rightarrow e \bar{\nu} + MET + \dots$ channel since it has
 203 the same underlying partonic process as in β -decay ($\bar{u}d \rightarrow e \bar{\nu}$). With the anticipated accuracy
 204 of about 5×10^{-4} for the transverse electron polarization related correlation coefficients in the
 205 BRAND experiment one would obtain significantly tighter bounds on the real and imaginary
 206 parts of scalar and tensor coupling constants and, consequently, on ϵ_S and ϵ_T as shown in
 207 Figure 15.5. It should be noted that such limits would be competitive to those extracted from
 208 the analysis of 20 fb^{-1} CMS collaboration data collected at 8 TeV [26, 27] and even to the
 209 planned measurements at 14 TeV.

210 Acknowledgments

211 This work has been supported in part by The National Science Centre, Poland, under the grant
 212 No. 2018/29/B/ST2/02505.

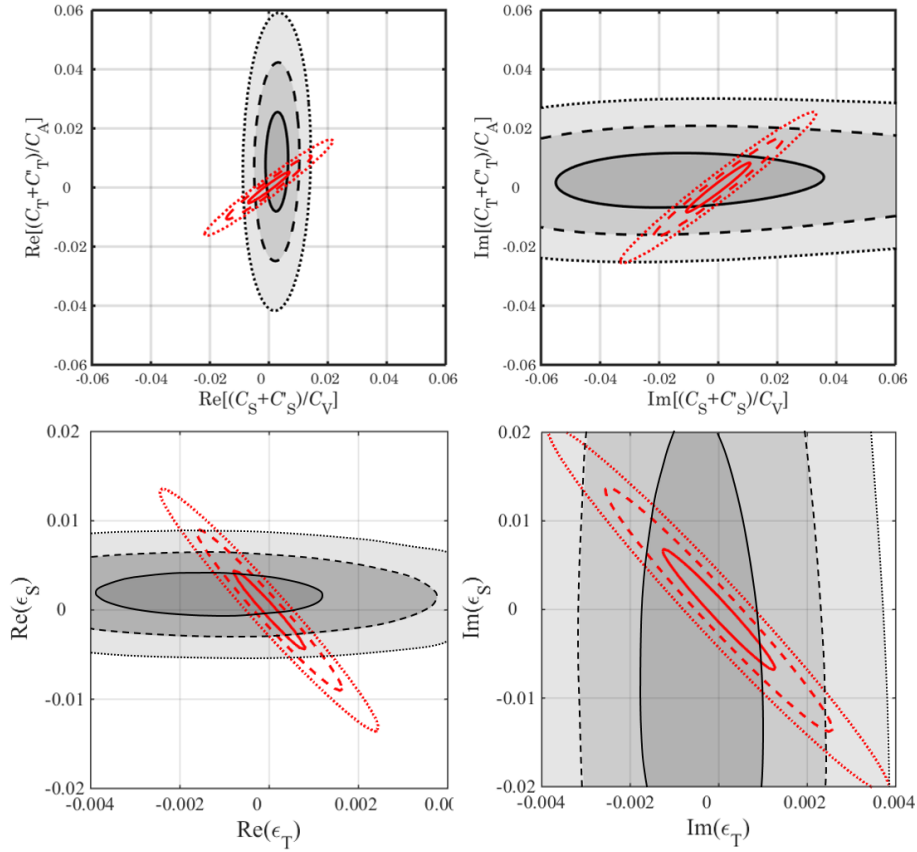


Figure 15.5: Experimental bounds on the scalar vs. tensor couplings \mathfrak{S} , \mathfrak{T} from (15.2) (upper panels) and translated to EFT parameters ϵ_S , ϵ_T (lower panels) published in [23]. The gray areas represent the information deduced from available experiments as listed in [24], while the red lines represent the limits resulting from the correlation coefficients H , L , N , R , S , U and V measured with the anticipated accuracy of 5×10^{-4} . Solid, dashed and dotted lines correspond to 1-, 2- and 3- σ confidence levels, respectively, in analogy to decreasing intensity of the grey areas.

213 References

- 214 [1] J. H. Christenson *et al.*, *Evidence for the 2π decay of the K_2^0 meson*, Phys. Rev. Lett. **13**,
215 138 (1964).
- 216 [2] K. Abe *et al.*, *Improved measurement of mixing-induced CP violation in the neutral B meson*
217 *system*, Phys. Rev. D **66**, 071102 (2002).
- 218 [3] P. Vogel and B. Werner, *Final-state interactions and time-reversal tests in nuclear β -decay*,
219 Nuclear Physics A **404**, 345 (1983).
- 220 [4] A. N. Ivanov *et al.*, *Test of the Standard Model in Neutron Beta Decay with Polarized Electron*
221 *and Unpolarized Neutron and Proton*, Phys. Rev. D **99**, 053004 (2019).
- 222 [5] A. N. Ivanov *et al.*, *Corrections of order $O(E_e^2/m_N^2)$, caused by weak magnetism and pro-*
223 *ton recoil, to the neutron lifetime and correlation coefficients of the neutron beta decay*,
224 arXiv:2010.14336 [hep-ph] (2020).

- 225 [6] N. Danneberg *et al.*, *Muon Decay: Measurement of the Transverse Polarization of the Decay*
226 *Positrons and its Implications for the Fermi Coupling Constant and Time Reversal Invariance*,
227 *Phys. Rev. Lett.* **94**, 021802 (2005).
- 228 [7] M. Abe *et al.*, *New Limit on the T-Violating Transverse Muon Polarization in $K^+ \rightarrow \pi^0 \mu^+ \nu$*
229 *Decays*, *Phys. Rev. Lett.* **93**, 131601 (2004).
- 230 [8] R. Huber *et al.*, *Search for Time-Reversal Violation in the β Decay of Polarized ^8Li Nuclei*,
231 *Phys. Rev. Lett.* **90**, 202301 (2003).
- 232 [9] J. D. Jackson *et al.*, *Possible Tests of Time Reversal Invariance in Beta Decay*, *Phys. Rev.*
233 **106**, 517 (1957).
- 234 [10] P. A. Zyla *et al.*, *Particle Data Group*, *Prog. Theor. Exp. Phys.* **2020**, 083C01 (2020).
- 235 [11] J. Zejma *et al.*, *FUNSPIN polarized cold-neutron beam at PSI*, *Nucl. Instr. Meth. Phys. Res.,*
236 *Sect. A* **539**, 622 (2005).
- 237 [12] G. Ban *et al.*, *A Mott polarimeter for the search of time reversal violation in the decay of*
238 *free neutrons*, *Nucl. Instr. Meth. Phys. Res., Sect. A* **565**, 711 (2006).
- 239 [13] A. Kozela *et al.*, *Measurement of the Transverse Polarization of Electrons Emitted in Free-*
240 *neutron Decay*, *Phys. Rev. Lett.* **102**, 172301 (2009).
- 241 [14] S. Agostinelli *et al.*, *Geant4 – a simulation toolkit*, *Nucl. Instr. Meth. Phys. Res., Sect. A*
242 **506**, 250 (2003).
- 243 [15] F. Salvat *et al.*, *ELSEPA – Dirac partial-wave calculation of elastic scattering of electrons and*
244 *positrons by atoms, positive ions and molecules*, *Comp. Phys. Comm.* **165**, 157 (2005).
- 245 [16] M. A. Khakoo *et al.*, *Monte Carlo studies of Mott scattering asymmetries from gold foils*,
246 *Phys. Rev. D* **64**, 052713 (2001).
- 247 [17] A. Kozela *et al.*, *Thickness scan of metallic layer by photon induced X-ray emission*, *Nucl.*
248 *Instr. Meth. in Phys. Res., Sect. B* **269**, 1767 (2010).
- 249 [18] A. Kozela *et al.*, *Measurement of the transverse polarization of electrons emitted in free*
250 *neutron decay*, *Phys. Rev. C.* **85**, 045501 (2012).
- 251 [19] N. Severijns *et al.*, *Tests of the standard electroweak model in beta decay*, *Rev. Mod. Phys.,*
252 *Sect. A* **78**, 991 (2006).
- 253 [20] P. Herczeg, *Beta decay beyond the standard model*, *Prog. Part. Nucl. Phys.* **46**, 413 (2001).
- 254 [21] J. Sromicki, *T Violation in the weak scalar and tensor interaction: neutron and nuclei*,
255 *Nucl. Instr. Meth. in Phys. Res., Sect. A* **440**, 609 (2000).
- 256 [22] K. Bodek, *R- and N-correlation coefficients in neutron decay: Search for scalar and tensor*
257 *couplings in weak interactions*, *Physics Procedia* **17**, 30 (2011).
- 258 [23] K. Bodek *et al.*, *BRAND: Search for BSM physics at TeV scale by exploring transverse po-*
259 *larization of electrons emitted in neutron decay*, *EPJ Web of Conferences* **219**, 04001
260 (2018).
- 261 [24] M. Gonzalez-Alonso *et al.*, *New physics searches in nuclear and neutron β decay*, *Prog.*
262 *Part. Nucl. Phys* **104**, 165 (2019).

- 263 [25] O. Naviliat-Cuncic *et al.*, *Prospects for precision measurements in nuclear β decay in the*
264 *LHC era*, *Ann. Phys.* **525**, 600 (2013).
- 265 [26] S. Chatrchyan and others (CMS Collaboration), *Search for new physics in events with*
266 *same-sign dileptons and b-tagged jets in pp collisions at $s = 7$ TeV*, *JHEP* **1208**, 023 (2012).
- 267 [27] V. Khachatryan and others (CMS Collaboration), *Search for physics beyond the standard*
268 *model in final states with a lepton and missing transverse energy in proton-proton collisions*
269 *at $s = 8$ TeV*, *Phys. Rev. D* **91**, 092005 (2015).